(Received 3 January 2026, Accepted 27 February 2026, Scheduled 19 April 2026)

Cluster Driven Subarray Setup for Reinforcing Phased Beam Pattern: A Comparative Analysis for Four Array Grids

Randa Y. Hussein and Ahmed J. Abdulqader*

College of Electronics Engineering, Ninevah University, Mosul, Iraq

ABSTRACT: This paper aims to propose efficient scenarios for constructing subarray structures based on innovative cluster configurations for high-performance beamforming. Two efficient methods, spatial assembly clustered subarray (SACS) and radial section clustered subarray (RSCS), are proposed for constructing multiple planar antenna arrays. Several array grid shapes were selected, including the rectangular array (RA), uniformly circular area randomly filling (UCARF), polycycle concentric array (PCA), and circular rectangle lattice array (CRLA). Synthesizing large arrays requires a high-performance algorithm to ensure error-free tuning. Therefore, the optimization process was assigned to the convex optimization (CO) algorithm. A set of radiation constraints was incorporated to generate a strong phased beam pattern (PBP) based on the innovative cluster structures, including steering and null steering, and a significant reduction in the sidelobe levels (SLLs). Complex excitation optimization of the subarray elements was used to meet the requirements of electromagnetic radiation. Simulation results show that the four topologies using the RSCS method offer better control than the SACS method in terms of reducing the SLL. The CRLA-RSCS method achieved -82.6 dB, the CRLA-SACS of -60 dB, the UCARF-RSCS of -45 dB, the PCA-RSCS of -39 dB, and the RA-RSCS method of -35 dB, with the other subarrayed array methods achieving -30 dB. Regarding the null steering characteristic, the CRLA-SACS method achieved a better depth, reaching -150 dB, than the other clustered array tiling methods. In all the proposed configurations, the main beam was steered at a 30-degree angle and could be reconfigured as required. Therefore, the design of such antenna arrays makes them suitable for modern and future communication applications.

1. INTRODUCTION

Phased array antenna system is used in many modern communication applications, such as 5G and beyond, and radar [1–3]. The operating strategies of these applications require antennas with high gain efficiency and efficient steering range, along with a very high drop in the SLLs in their transmitting and receiving units. For example, some modern radar systems require high-directional beams and variable-band scanning antennas to ensure the detection of the desired target without generating dead zones [4]. For this reason, there is a necessary need for an antenna system with high flexibility in its radiation performance in terms of the main beam steering and the wavelength spacing between the radiating elements. However, increasing the size of the radiating elemental antenna system creates significant problems in terms of power feeding network design (high system cost), which requires feeding each element individually, both amplitude and phase [5]. To address such problems, several efficient simplification techniques have been proposed, the most important of which is dividing a large array into co-feeding element clusters, which is called the subarray technique. This approach is based on reducing the number of transmit/receive chain units, which are responsible for the complexity of the system in practice.

Recently, steered subarrays have been discussed remarkably [6–9]. Such subarrayed arrays are characterized by greatly reducing the number of transmit/receive (T/R) units by making the radiating elements into unified groups that share a single channel, thus reducing complexity and cost. For phase-specific subarrays, non-periodicity in the arrangement of clusters is very important to avoid the generation of troublesome SLL that may reduce the efficiency of radiation steering. Based on this, two types of methods for achieving non-periodic SLL have been proposed by the researchers. The first method involves arranging the subarrays by creating irregular and rounded shapes [10–14], while the second method involves non-periodic phase feeding [15]. Although a beam can be directed with high efficiency by designing irregular subarrays, it leads to significant design complexity due to the huge number of radiating assemblies. In [16], reducing the complexity of an antenna system by using similar and repeating clusters was proposed. Anyway, the use of such a subarrayed array is limited and restricted because it takes the form of fixed clusters. However, designing subarrays with different internal feeds in terms of amplitude and phase can provide an efficient beam scope while reducing system complexity [17]. In [15], partial-directed arrays were designed in terms of cluster composition and varied feeding to achieve a wide coverage range in the azimuth axis. In all the previously proposed approaches, the authors attempted to achieve both phased and unphased beam patterns while optimizing the electromagnetic performance requirements of the antenna system. As mentioned earlier, the use of subarrays introduces problems in the generated pattern due to the aperiodicity of the SLL [18] and grating lobes [19]. To solve these prob-

* Corresponding author: Ahmed Jameel Abdulqader (ahmed.abdulqader@uoninevah.edu.iq).

lems, different tiling techniques were used and have proven their optimization efficiency [10]. The techniques used in the aforementioned research are the creation of different polyominos, a partially clustered array, a hybrid clustered array, and the tiling of a quarter of the square array with rotation to the remaining quarters. Synthesizing the steering main beam subarrays is a challenge among authors as it requires providing a highly steering beam and high SLL reduction with a few irregular clusters tiling to avoid systemic and computational complexity. Using clusters in large numbers requires the use of optimization algorithms with many iterations, which may result in a time cost that exceeds the acceptable range. A wide variety of optimization algorithms based on biological or mathematical methods have been developed to address such methods, including genetic algorithms, swarm intelligence, compressed sensing techniques, and others. However, as the number of clusters in the subarray increases, the computational efficiency of these algorithms deteriorates significantly, even though they have significantly improved the beam pattern, especially when the tiling process exhibits irregularities.

In this study, an efficient systematic strategy is presented for synthesizing two-type cluster tiling configurations on four types of 2D antenna arrays and comparing them, enabling the construction of high-performance antenna array systems. The proposed scenario integrates the framework for designing conventional and unconventional array grids with the creation of irregular and unconventional cluster substructures through adaptive distribution of excitation amplitudes and phases. The proposed method facilitates the synthesis of various antenna aperture grids, including RA, UCARF, PCA, and CRLA grids, by partitioning them using SACS and RSCS, enabling the provision of an adaptive electromagnetic radiation structure suitable for large and narrowband complex array systems.

The proposed method offers adaptive synthesis and dynamic control of a high-performance electromagnetic PBP in terms of beamforming and damping using the CO algorithm. Consequently, this combination results in easy beam direction with high-precision focusing at the required coverage angles. Simultaneously, the SLL power is dampened by interference signal suppression through the generation of deep zero regions. This optimal electromagnetic performance allows the designer to synthesize a flexible beamforming in terms of beam scanning with high efficiency across various subarrayed array apertures. Furthermore, the complex excitations of the proposed clustered arrays are flexibly controlled by a balanced dynamic distribution of the subarrays. The entire approach was supported by the MATLAB environment.

2. THEORY AND OPTIMIZATION MODEL PROCESS

Assume a 2D array matrix composed of $N \times M$ isotropic elements uniformly positioned (equal distance between any two successive elements) along the x and y axes. Each element in the array has an independently distinct excitation amplitude and phase. Based on the above, the hypothetical mathematical model for the array factor (F) of the 2D array can be expressed as follows [14]:

$$\mathrm{F}(u,v) = \sum_{n=1}^{N}\sum_{m=1}^{M} I_{nm} \exp\left(j\frac{2\pi}{\lambda}d((n-1)(u-u_o) + (m-1)(v-v_o))\right) \quad (1)$$

where I_{nm} is the complex (amplitude and phase) excitation; λ is the wavelength of the center frequency; $d = d_x = d_y = 0.5\lambda$, $u = \sin\theta\cos\phi$, and $v = \sin\theta\sin\phi$ are the elevation and azimuth planes, respectively; (u_o, v_o) refer to the steering main beam direction. To prepare the grid configuration for the 2D array, a mathematical equation is considered in terms of its standard spatial dimensions with respect to λ, which is defined as follows:

$$G = \{(x_n, y_m)\}_{n,m=1}^{NM} \subset R^2, \quad N \times M = |G| \quad (2)$$

Based on the parameter structure shown in Eq. (2), the array factor model enables the construction of various 2D arrays, such as rectangular, square, triangular, hexagonal, and circular configurations. However, to enable fair comparisons in terms of array dimensions, RA, UCARF, PCA, and CRLA array structures were constructed. The minimum bound integer is represented by the symbol $\lfloor\cdot\rfloor$. For each geometric grid, the space area of the array can be expressed using a mathematical model derived from the parameters specified in Eq. (2). The construction process begins by studying the RA grid configuration as shown in Fig. 1(a), where RA is constructed as follows:

$$\begin{aligned} x_{a,\,b} &= ad_x,\ a = 0, 1, \ldots, N-1 \\ y_{a,\,b} &= bd_y,\ b = 0, 1, \ldots, M-1 \end{aligned} \quad (3)$$

$$RA = N \times M \quad (4)$$

For the UCARF configuration as shown in Fig. 1(b), the radius (R) is defined as:

$$R = \frac{Nd_x(or\ Md_y)}{2} \quad (5)$$

It is specified at random angles (θ or $\phi \sim [0, 2\pi]$) within the radial coordinates (u, v) using a sampling limit in a regular circular space ($r_{n\,or\,m} = R\sqrt{u_n}$ or $\sqrt{v_m}$) as follows.

$$x_n = r_n\cos\theta_n \text{ or } y_m = r_m\sin\theta_m \quad (6)$$

As shown in Fig. 1(c), the PCA is defined as a regular concentric ring pattern of multiple circular rings that share the same geometric center with varying and symmetrical diameters. Mathematically, a polycycle can be expressed as a chain equation according to the number of rings as follows:

$$R_k = \left[r_k^2 = x_n^2 + y_m^2 | (x_n, y_m)\right] \quad (7)$$

where r_k^2 is the radius of the rings kth ring in the PCA ($r_{k+1} > r_k$). All elements in the rings are arranged equidistant from each other such that:

$$\gamma_{r_k,n\,or\,m} = \frac{2\pi n}{N_{r_k}} \text{ or } \frac{2\pi m}{M_{r_k}} \quad (8)$$

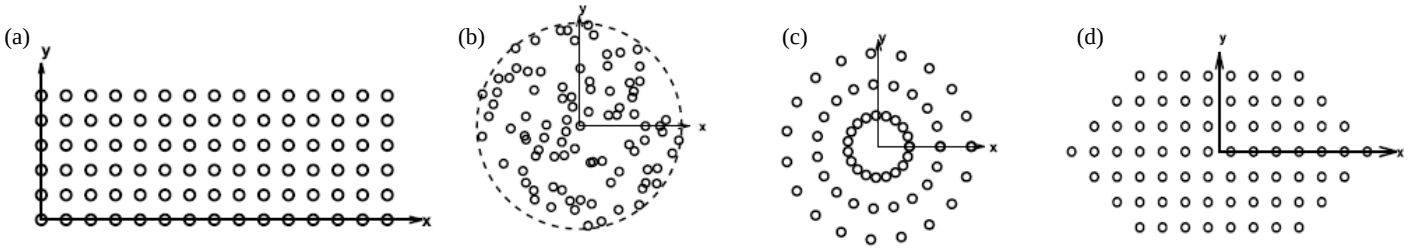

FIGURE 1. Imagination of the 2D array grids for the four topologies, (a) RA, (b) UCARF, (c) PCA, (d) CRLA.

So,

$$x_n = \bigcup_{r_k} r_k d_x \cos\gamma_{r_k,n} \text{ or } y_m = \bigcup_{r_k} r_k d_y \cos\gamma_{r_k,m} \tag{9}$$

Finally, the CRLA grid can be defined as a grid consisting of a set of points distributed over a surface area consisting of two vectors of equal length with an alternating angle of 60° (see Fig. 1(d)). This topology can be expressed mathematically as:

$$\begin{aligned} (x_n, y_m) &= (n_{dx} + m_{dy}) \\ (n_{dx})^2 + (m_{dy})^2 &\leq R^2 \end{aligned} \tag{10}$$

The electromagnetic radiation generated by the four array grids can be expressed using the array factor model in Eq. (1). In this model, the combination enables the construction of an undirected beam pattern by optimizing the excitation weights of the array elements individually (high complexity) while maintaining the inter-element spacing constant, as discussed above. From here, the idea of partitioning the array elements into smaller subarrays can be considered, which reduces the complexity of the overall antenna structure, both practically and computationally. An important consideration when synthesizing clustered arrays is to preserve the radial characteristics of the patterns, as in the case of fully synthesizing arrays. Carless partitioning can lead to undesirable engineering problems, such as the generation of prominent periodic SLL, formation of grating lobes, failure to generate null steering, and, most importantly, difficulties in steering the main beam to the required coverage angles under the constraints imposed by the clustered subarray structure. Accordingly, in this study, two types of subcluster partitions are proposed to encompass the geometric configurations of the four array grids. Let q be the number of cluster subarrays, which is adaptively determined by both the quantity and geometric configuration of the submatrices, and is expressed as follows:

$$\begin{aligned} &s : \{1, \ldots, N\}, \{1, \ldots, M\} \to \{1, \ldots, Q\}, \\ &s(n, m) = clustered\ subarray\ index\ of\ elements\ N \times M \end{aligned} \tag{11}$$

To establish clustered subarrays under different structural configurations, the centers of the subarrays were designated as follows:

$$\delta_q = \frac{1}{|S_q|} \sum_{n,m \in s_q} \begin{bmatrix} x \\ y \end{bmatrix}, \quad S_q = \{n \times m : s(n, m) = q\} \tag{12}$$

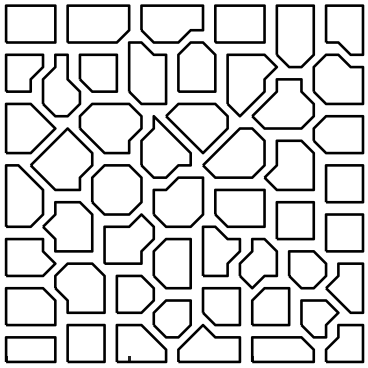

FIGURE 2. The suggested SACS architecture.

Two cluster splitting models, which include four array grids, are presented to facilitate the design of high-performance electromagnetic planar arrays capable of generating customized PBPs. In the first clustered subarray method, the main array elements are adaptively segmented into tightly packed subarray clusters based on the spatial proximity of the radiating elements. This can be referred to as SACS, as shown in Fig. 2. This segmentation ensures that the structural density of the element clusters is nearly equal, guaranteeing a largely balanced spatial coverage across the array aperture. Providing a stable performance of the radiated PBP against the random excitation distortions generated by the synthesis of regular clusters, as discussed in the Introduction. The SACS approach offers a stable and electromagnetically efficient pattern with the ability to be reconfigured as required. To achieve such radiation specifications, highly flexible dynamic subarrays must be constructed that precisely manage spatial variation and can be applied to various types of two-dimensional apertures. Then, the mathematical model of the SACS method can be represented as:

$$\min_{\{\delta_q\}, s(.)} \sum_{n=1}^{N} \sum_{m=1}^{M} \left\| [x, y]^T - \delta_{s(n,m)} \right\|_2^2 \tag{13}$$

A second partitioning method based on radial plane shapes with varying radial distributions, called RSCS, was considered. In this architecture, the partitioning process relies on spatial configurations, where subarrays are constructed by arranging elements into expanding diffusion clusters. These clusters were partitioned according to the type of aperture in the array, either diffusion from the center to the edges or from the bottom to the top, as illustrated in Fig. 3. This architecture provides coherent angular diffusion cluster structures in the ar-

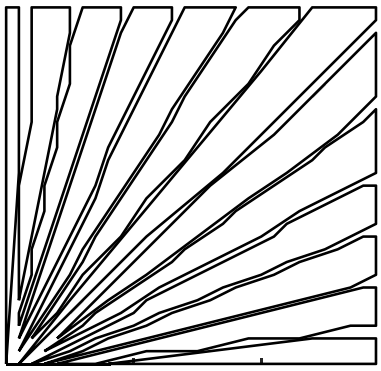

FIGURE 3. The suggested RSCS architecture.

rangement of radiating elements based on the principle of radial diffusion, thus offering adaptive flexibility in synthesizing radial coverage patterns. This leads to the generation of unequal cluster sizes with irregular spatial densities, particularly near the edges of the aperture. To illustrate this principle, let $\beta_{nm} = a\tan 2(x, y) \in [0, 2\pi)$, then:

$$s(n, m) = \left\lceil Q\frac{\beta_{nm}}{2\pi} \right\rceil \tag{14}$$

Once one of the 2D array grids and one of the two cluster subarray block types are identified, the two structures are combined through a unified array factor model, which is then incorporated into the excitation optimization process. As previously mentioned, $Q \in R^{N\times M}$, where:

$$Q_{xy} = \begin{cases} 1, & if\ the\ elements\ n \times m\ belongs\ to\ subarray\ S_q \\ 0, & otherwise \end{cases} \tag{15}$$

Accordingly, the matrix representing the effective cluster weights is expressed as:

$$I^Q_{nm} = |I_Q| \cdot |I_{nm}|, |I_Q| \in \mathrm{C}^Q \tag{16}$$

Eq. (16) is combined with Eq. (1) to enable the synthesis of a clustered subarray-based array grid structure within the real-time optimization process. To achieve effective control of the generated PBP, an array factor model is designed with a set of control constraints that force the generated electromagnetic pattern to steer the main beam in the desired direction with high directivity, significantly reduce SLLs in other directions, and impose wide and deep zero null-steering in specific directions during the real-time optimization process. The main beam is assumed to be directed along $(u_{bs}, v_{bs}) = (\theta_{bs}, \phi_{bs})$ with a half of $BW/2$, such that the main beam orientation can be represented in terms of the angular parameters (θ, ϕ) as:

$$\begin{aligned} \theta_{bs} &= [\theta_{bs} - BW/2,\ \theta_{bs} + BW/2] \\ \phi_{bs} &= [\phi_{bs} - BW/2,\ \phi_{bs} + BW/2] \end{aligned} \tag{17}$$

During the array optimization process, a specific parameter, BW, was fixed to regulate the width of the main beam, whereas the SLL was constrained by the specifications along the elevation and azimuth axes, assuming that the two axes were symmetrical as follows:

$$\begin{aligned} \theta_{SLL} &= \{\theta : \theta \le \theta_{bs} - BW/2 - \xi\} \cup \{\theta : \theta \ge \theta_{bs} + BW/2 + \xi\} \\ \phi_{bs} &= \{\phi : \phi \le \phi_{bs} - BW/2 - \xi\} \cup \{\phi : \phi \ge \phi_{bs} + BW/2 + \xi\} \end{aligned} \tag{18}$$

Here, ξ denotes the prescribed SLL that must be attained in the synthesized PBP. The zero null-direction strict, on the other hand, is determined by forcing the array operator to be zero (i.e., $\mathrm{F}(u_{ns}, v_{ns}) = 0$), as expressed by:

$$\mathrm{F}(u_{ns}, v_{ns}) = [\mathrm{F}(\theta_{ns}, \phi_{ns})] \in N \times M \tag{19}$$

Ultimately, the task of synthesizing the above mathematical settings and concepts is assigned to the CO algorithm as follows:

$$\mathrm{F}(u, v)_{final} = a(u, v)\left\{I^Q_{nm}\right\}^H \tag{20}$$

where $a(u, v) = \exp(j\frac{2\pi}{\lambda}d((n-1)(u-u_o)+(m-1)(v-v_o)))$. The final normalization of Eq. (20) can be expressed in dB scale as:

$$\mathrm{F}(u, v)_{\mathrm{dB}} = 20\log\frac{\mathrm{F}(u, v)_{final}}{\max|\mathrm{F}(u, v)_{final}|} \tag{21}$$

The proposed strategy aims to formulate a compliant PBP formation problem based on the three required constraint behaviors (main beam steering, SLL reduction, and deep and wide null steering) as an advanced model that provides a solution to the array pattern performance problem.

$$\begin{aligned} &\underset{I^Q_{nm}}{\text{maximize}}\ \ell \\ &\textit{subject to:}\ \Re(\left\{I^Q_{nm}\right\}^H a(u_{bs}, v_{bs})) \ge \ell,\ \forall(\theta, \phi) \in (\theta_{bs}, \phi_{bs}) \\ &\qquad \left|\left\{I^Q_{nm}\right\}^H a(u_{SLL}, v_{SLL})\right| \le \xi,\ \forall(\theta, \phi) \in (\theta_{SLL}, \phi_{SLL}) \\ &\qquad \left|\left\{I^Q_{nm}\right\}^H a(u_{ns}, v_{ns})\right| \le \psi,\ \forall(\theta, \phi) \in (\theta_{ns}, \phi_{ns}) \\ &\qquad \left\|I^Q_{nm}\right\|_2 \le 1 \end{aligned} \tag{22}$$

where $SLL = 10^{-\frac{\xi}{20}}$ and $ns = 10^{-\frac{\psi}{20}}$. $\|I^Q_{nm}\|_2 \le 1$ indicates the threshold value allocated to express the total input power of the clustered subarray elements.

3. SIMULATION RESULTS

To demonstrate the significance and effectiveness of the proposed approach, assume the initial use of an RA with 30×40 elements evenly distributed along the two axes. This array was then subdivided into two proposed subarrays, RA-SACS and RA-RSCS. The design of the other array apertures was then considered to construct the following configurations: UCARF-SACS, UCARF-RSCS, PCA-SACS, PCA-RSCS, CRLA-SACS, and CRLA-RSCS. In all the proposed optimized configurations, complex excitation optimization was employed to achieve the best possible electromagnetic performance. Likewise, all combinations adhered to the constraints imposed by the algorithm as follows: $(\theta_{bs}, \phi_{bs}) = (30°, 30°)$,

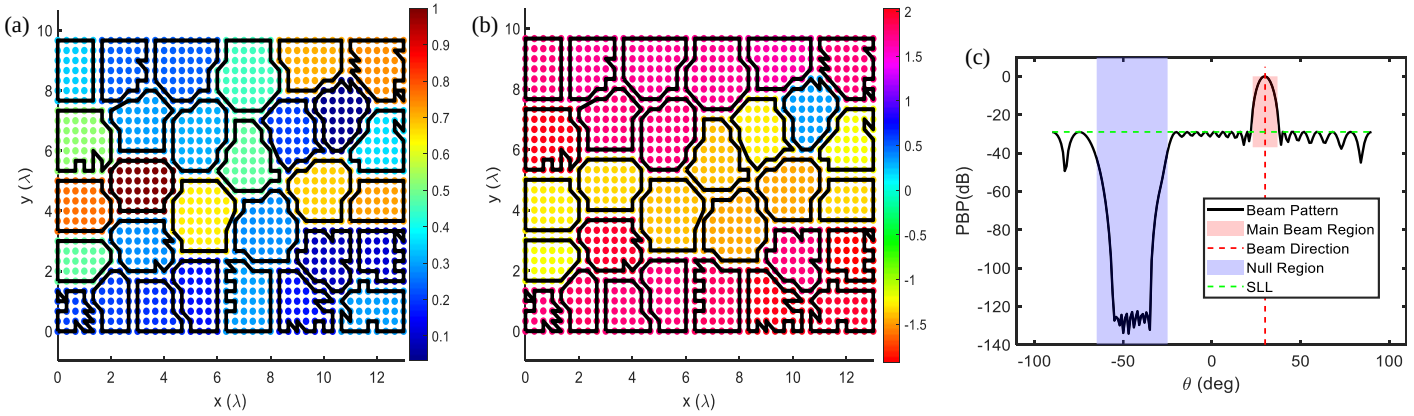

FIGURE 4. Numerical computing investigation: results of test 1 (RA with SACS), (a) amplitude clusters distribution, (b) phase clusters distribution, (c) PBP.

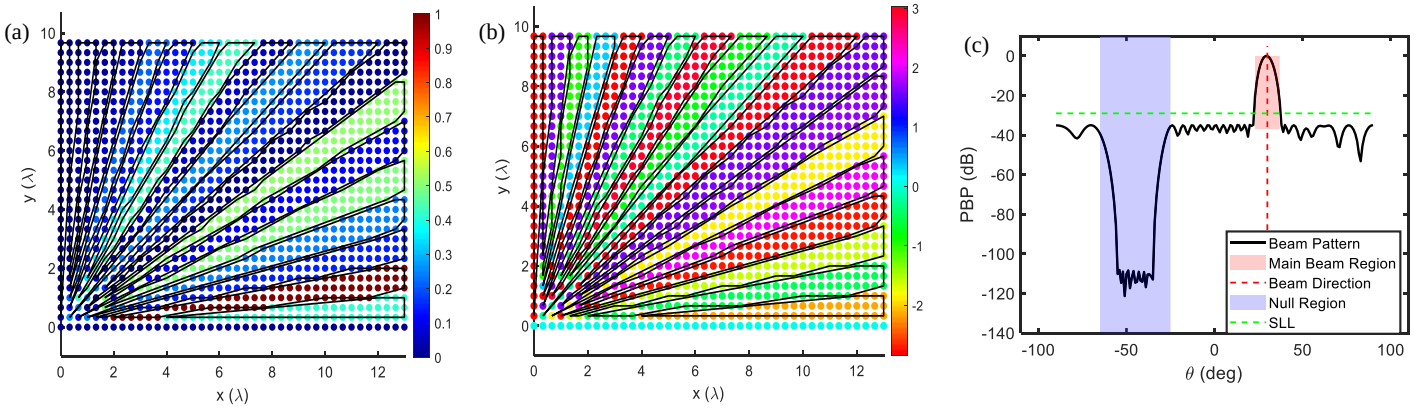

FIGURE 5. Numerical computing investigation: results of test 1 (RA with RSCS), (a) amplitude clusters distribution, (b) phase clusters distribution, (c) PBP.

$\xi = -30$ dB, $BW = 5$, and 50° of null steering of 20 width and -120 dB deep. These constraints are used as reference characteristics to achieve a high-performance PBP and perform a comparative analysis across the four array grid configurations under the proposed cluster block structures. A series of empirical trials were performed based on the number of synthesized structures, with each structure being executed multiple times to confirm the validity of the proposed method for synthesizing the constrained PBP resulting from the tiling of the proposed subarray structures. To clarify the vision and interpretation of the results in all scenarios, the resulting PBP from the combinations was plotted on two axes (azimuth axis) rather than three axes.

Test1: First, the SACS method was applied to the RA as shown in Fig. 2. Based on the initial configuration, this architecture presents a homogeneous cluster distribution model. Within the constraints imposed by the algorithm, this architecture demonstrated its ability to adapt to these limitations, resulting in precise main beam orientation of 30° with a beamwidth of approximately 5°, SLL of -30 dB, null steering at $-50°$ with a beamwidth of 20°, and a depth of approximately -139 dB (see Fig. 4). Owing to the intelligent and homogeneous distribution of the subarrays, spatial distributional balance was achieved among the elements within the clusters, with no overlap or any element being excluded from any cluster within the main aperture boundaries. In contrast, the RSCS architecture offers better control of the constraints by maintaining the orientation of the main beam and reducing the SLL by 5 dB for the same aperture (see Fig. 5). Regarding the zero-null depth, the first method had greater control than the second, generating a depth 19 dB deeper.

RSCS reduced the dispersion of the SLLs by 5 dB compared with that of the SACS. This reduces the spatial adaptability of the clustered subarrays but enhances the PBP accuracy within the specified corner compartments. Therefore, SACS pooling demonstrated the ability to generate a significantly deeper null region spatially, achieving significant destructive interference and enhancing interference signal attenuation to a depth of -139 dB. The second clustered subarray, RSCS, produced mostly constant angular profiles in specific directions, thus providing slightly wider gap regions in the PBP than the first method, resulting in narrower suppression zones. The SACS configuration provided a deeper null region, demonstrating an improvement in the strong null depth for the same direction of approximately 19 dB compared to the RSCS.

Test 2: As shown in Fig. 6, the UACRF, which uses SACS, provides an improved adaptive capacity for forming random clusters within the grid overlay based on the complex feeding of each cluster, allowing greater cluster configuration flexibility in the spatial assembly of the array topology. Despite the random

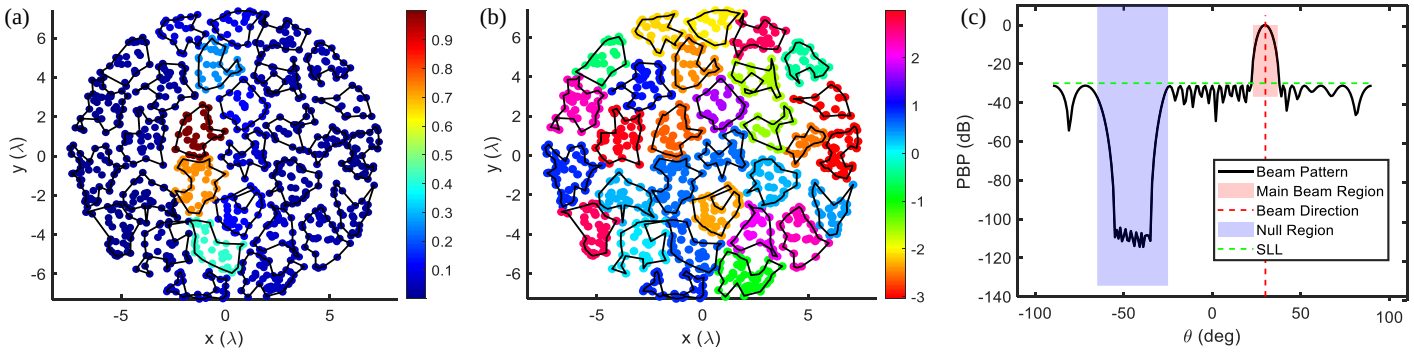

FIGURE 6. Numerical computing investigation: results of test 2 (UACRF with SACS), (a) amplitude clusters distribution, (b) phase clusters distribution, (c) PBP.

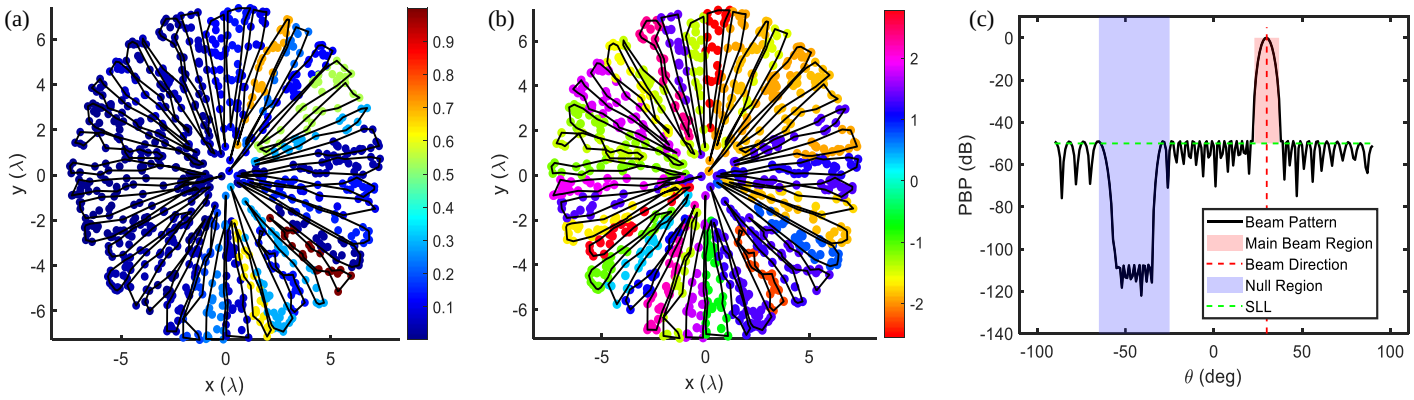

FIGURE 7. Numerical computing investigation: results of test 2 (UACRF with RSCS), (a) amplitude clusters distribution, (b) phase clusters distribution, (c) PBP.

arrangement of elements within the aperture and the subsequent random arrangement of clusters, this approach demonstrated its ability to handle the strict constraints imposed by the algorithm, reducing the level of the imposed sidelobes to -31 dB. It also provided the necessary protection for the main beam against distortions resulting from the random distribution of elements and clusters.

In the second architecture, because the target aperture is circular, the longitudinal angular clusters are formed as rays emanating from the center of the array to its edges, resulting in subarrays that are different from those of square and rectangular apertures. It gives the array a distinctive geometric configuration, as shown in Fig. 7. This combination resulted in an arrow-shaped spatial distribution of elements, including the clustering of different excitation weights within a cluster. This arrangement of elements was better than that of the first method, significantly reducing random distances. Therefore, a high-performance pattern was formed, particularly in terms of reducing the SLL to more than -45 dB (approximately 15 dB compared to the first method), while maintaining other constraints. This improvement is attributed to the similarity of the amplitude and phase excitation cluster structures in terms of geometric distribution, in addition to the lower complexity of the cluster structure.

Test 3: In this test, the elements in the clusters were arranged as circular, uniformly contained, randomly arranged spatial blocks (i.e., SACS) within PCA. This resulted in a PBP with electromagnetic performance that perfectly met the algorithm's constraints, as shown in Fig. 8. Conversely, the second cluster architecture (i.e., RSCS) imposed a mostly linear cluster arrangement, leading to a pattern that exceeded the constraints in terms of the SLL, achieving a reduction of -40 dB while maintaining the other properties as specified, as shown in Fig. 9. This method exhibited minimal scattering in the element distribution, as some elements were left without clustering, particularly in areas far from the center. However, the number of scattering elements was fewer than the total number of elements in the array. This could be a drawback from the design of the feeding network, as each element requires individual synthesis away from the cluster feeds. However, this can be mitigated by disabling them (i.e., setting them off) since they carry a lower excitation weight than elements near the center.

Test 4: In this case, as in the other structures, the elements were arranged according to the proposed cluster structures, as shown in Figs. 10 and 11. These structures produced a high-performance PBP that far surpassed those of the other structures. The CRLA-SACS achieved an SLL of -60 dB and a null depth of -120 dB, whereas the CRLA-RSCS achieved a reduction of -82.6 dB SLL with a null depth of -150 dB. This superiority stems from the dynamic structure of the hexagonal topology, which combines the distribution of elements in square, rectangular, circular, and triangular shapes.

To demonstrate the robustness of the proposed cluster synthesis methods, the obtained results were compared with each

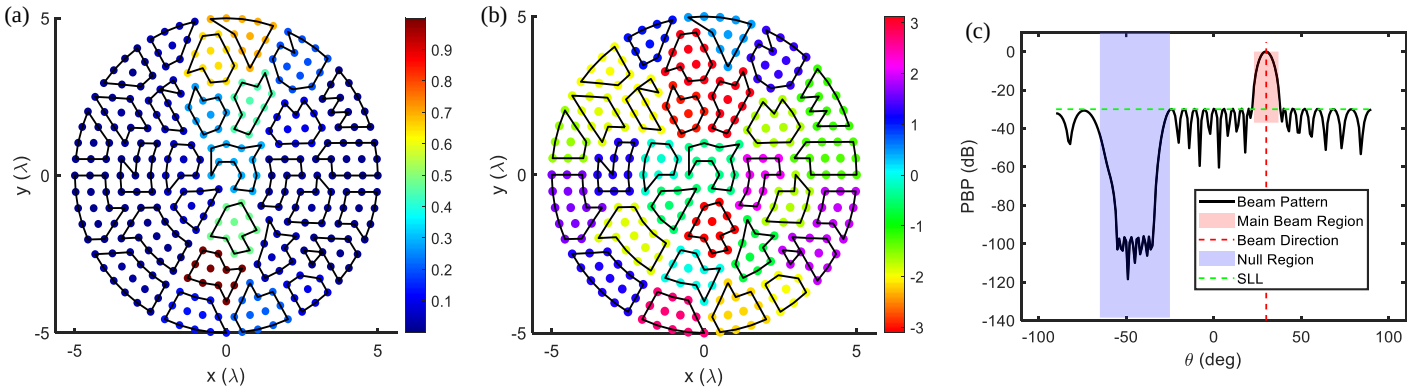

FIGURE 8. Numerical computing investigation: results of test 3 (PCA with SACS), (a) amplitude clusters distribution, (b) phase clusters distribution, (c) PBP.

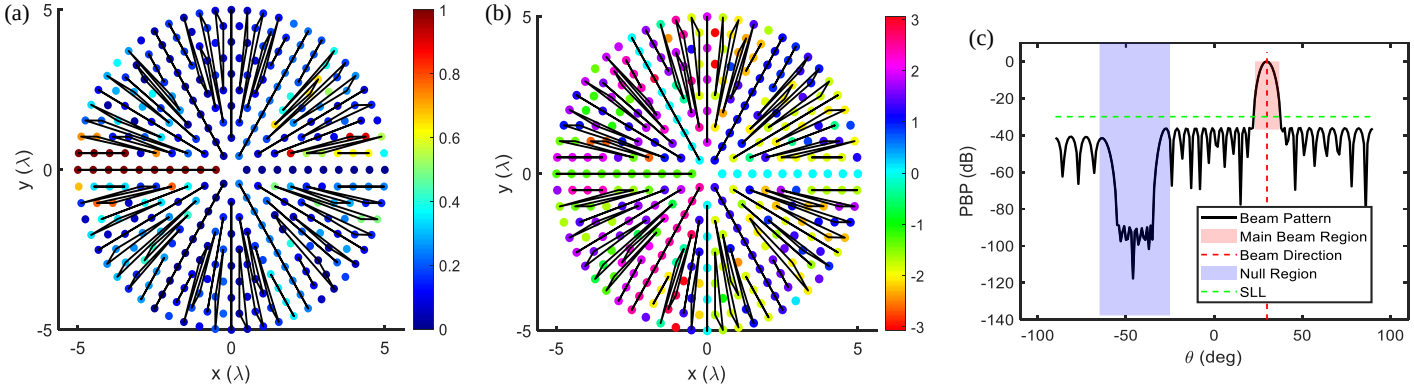

FIGURE 9. Numerical computing investigation: results of test 3 (PCA with RSCS), (a) amplitude clusters distribution, (b) phase clusters distribution, (c) PBP.

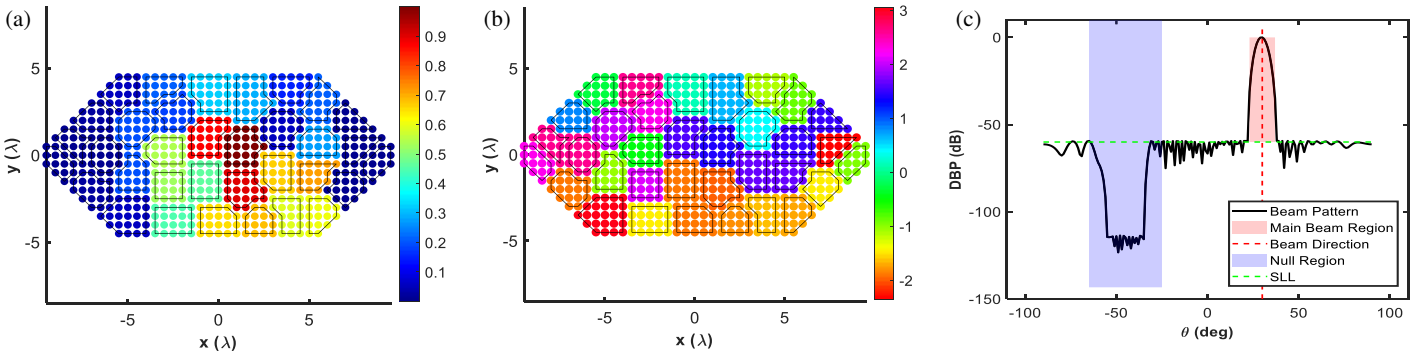

FIGURE 10. Numerical computing investigation: results of test 4 (CRLA with SACS), (a) amplitude clusters distribution, (b) phase clusters distribution, (c) PBP.

other and with results obtained from other literature studies [15, 20–23], as shown in Table 1. The comparison was based on several different subarray synthesis scenarios and considered design and radial characteristics such as antenna system complexity (number of feeding network components), beam orientation, SLL reduction, null orientation, and the type of algorithm used. Based on the comparison parameters shown in the table, the advantages of the proposed approaches can be seen in terms of design simplicity and efficient results. Some literature, as shown in [15, 20, 21], relied on optimizing a single excitation (amplitude or phase) in the clustered subarray synthesis process, achieving results in reducing the SLL by values ranging from -18 to -28.25 dB. However, in terms of reducing system complexity, Ref. [20] achieved a reduction of only 1.6%. This percentage is very small (and a very ideal case), but it was achieved at the expense of the SLLs, resulting in a slight reduction compared to the other references. This is because the degrees of freedom in the algorithm used were affected, negatively impacting the resulting pattern, since dealing with subarrays requires highly sophisticated geometric calculations. The

TABLE 1. Performance comparsion between the proposed methods and related studies work.

Ref.	Array type	Array element size	Clustered subarray type	Number of subarrays	Excitation type	Complexity (%)	Optimization algorithm type	Main beam steering?	SLL (dB)	Null steering	
										Width (Deg.)	Deep (dB)
[15]	Square	32×32	Tetromino subarrays	49	Phase only	9.6	Invasive weed optimization (IWO)	yes	-18	-	-
[20]	Square	35×35	K-means	10	Amplitude only	1.6	ISODATA	No	-28.3		
[21]	Square	20×20	Nonuniform	122	Phase only	61	Local and global	yes	-20	-	-
[22]	Square	12×12	Polyomino (L and T) shaped	10	Complex	27.7	Algorithm X	yes	-18	-	-
[23]	Rectangular	22×12	Irregular domino-shaped	231	Complex	43	GA	yes	-18.8	-	-
[this work]	RA	40×30	SACS	30	Complex	6.6	CO	yes	-30	30	-139
[this work]	RA	40×30	RSCS	30	Complex	6.6	CO	yes	-35	30	-120
[this work]	UACRF	900 elements	SACS	30	Complex	6.6	CO	yes	-30	30	-119
[this work]	UACRF	900 elements	RSCS	30	Complex	6.6	CO	yes	-45	30	-119
[this work]	PCA	900 elements	SACS	30	Complex	6.6	CO	yes	-30	30	-120
[this work]	PCA	900 elements	RSCS	30	Complex	6.6	CO	yes	-39	30	-120
[this work]	CRLA	900 elements	SACS	30	Complex	6.6	CO	yes	-60	30	-120
[this work]	CRLA	900 elements	RSCS	30	Complex	6.6	CO	yes	-82.6	30	-120

solution to this negative impact was to synthesize complex excitations when constructing clusters. This is observed in [22, 23], although they did not fully utilize this processing. The available results in these two references were around -18.4 dB as an average value, along with a systemic complexity of 43% in Ref. [23]. Another important factor affecting the results of [23], which did not allow for the full exploitation of the availability of complex trigger enhancement, is its use of a GA that requires high computational settings and presents algorithmic convergence challenges. In addition, a very important factor that previous literature has not considered is the null steering generation process.

High-performance radiation was achieved in the proposed scenarios. Unlike the literature listed in the table, a convex mathematical algorithm was used with cluster synthesis methods to produce the desired pattern under strict constraints. Comparing the results of previous studies with those of all methods used in this study, the proposed cluster structures demonstrated their robustness in achieving the imposed radiation characteristics with high precision. Under the constraints outlined in Eq. (21), all methods achieved the main beam orientation at 30° with the possibility of reorientation in any desired direction. Regarding the sidelobe leveling characteristic, the CRLA-RSCS method achieved the best SLL reduction at -82.6 dB, followed by the CRLA-SACS structure at -60 dB. Other methods, such as the UACRF-RSCS structure, achieved -45 dB, whereas the remaining methods ranged between -30 and -39 dB.

Regarding the zero-zone orientation (null steering) characteristic, the CRLA-RSCS structure achieved a depth of approximately -150 dB, the RA-SACS structure approximately -139 dB, and -120 dB in the other cases, along with a zero-zone width of 30° for all the methods. Regarding systemic complexity, all methods achieved very low levels despite the use of complex excitations in the synthesis process, with a complexity percentage of 6.6% across all proposed methods.

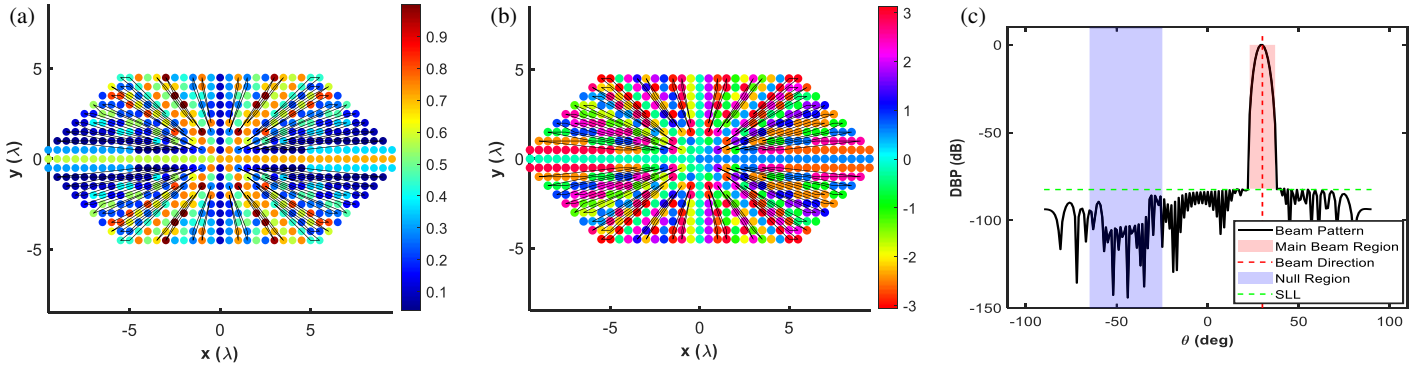

FIGURE 11. Numerical computing investigation: results of test 4 (CRLA with RSCS), (a) amplitude clusters distribution, (b) phase clusters distribution, (c) PBP.

4. CONCLUSION

This study proposes two novel approaches for robust subdivision cluster structures, SACS and RSCS, for slicing four different types of known array aperture grids: RA, UACRF, PCA, and CRLA grids. In all composite array grids, the RSCS method outperformed the SACS method in achieving high pattern performance due to its spatial distribution property based on a radial distribution. The proposed structures are built upon strict radial specifications, such as main beam steering, significant reduction of SLLs, and highly efficient zero-zone steering, in conjunction with an efficient optimization algorithm such as CO. All structural scenarios successfully met the strict constraints, and some methods significantly exceeded these constraints, as shown in the simulation results section. Regarding radial steering, all subarrayed arrays adhered to this constraint with negligible distortion. The results regarding the reduction in SLLs varied among the clustered constructs. The CRLA-RSCS method achieved a reduction of -82.6 dB, whereas the CRLA-SACS method achieved -60 dB, with lower reductions in the other methods. Conversely, regarding the zero null-direction properties, the CRLA-RSCS method achieved a depth of -150 dB, compared to -120 dB in the other methods. Furthermore, all the constructs adhered to a 30° null steering width, which is a crucial characteristic for precise applications that is difficult to achieve in subarrayed array synthesis. The most important aspect of these proposed methods is achieving a very low systemic complexity (low cost) compared to previous studies, as shown in Table 1. The design of such constructs (all subarrayed array grid cases) is innovative and meets the requirements of modern communications, e.g., 5G, radar for high-performance beamforming.

REFERENCES

[1] Mou, L. W., Y. J. Cheng, Y. F. Wu, M. H. Zhao, and H. N. Yang, "Design for array-fed beam-scanning reflector antennas with maximum radiated power efficiency based on near-field pattern synthesis by support vector machine," *IEEE Transactions on Antennas and Propagation*, Vol. 70, No. 7, 5035–5043, 2022.

[2] Herd, J. S. and M. D. Conway, "The evolution to modern phased array architectures," *Proceedings of the IEEE*, Vol. 104, No. 3, 519–529, 2016.

[3] Sun, J. X., Y. J. Cheng, and Y. Fan, "Planar ultra-wideband and wide-scanning dual-polarized phased array with integrated coupled-Marchand balun for high polarization isolation and low cross-polarization," *IEEE Transactions on Antennas and Propagation*, Vol. 69, No. 11, 7134–7144, 2021.

[4] Low, K. K. W., S. Zihir, T. Kanar, and G. M. Rebeiz, "A 27-31-GHz 1024-element Ka-band SATCOM phased-array transmitter with 49.5-dBW peak EIRP, 1-dB AR, and ±70° beam scanning," *IEEE Transactions on Microwave Theory and Techniques*, Vol. 70, No. 3, 1757–1768, 2022.

[5] Sun, G., Y. Liu, S. Liang, A. Wang, and Y. Zhang, "Beam pattern design of circular antenna array via efficient biogeography-based optimization," *AEU — International Journal of Electronics and Communications*, Vol. 79, 275–285, 2017.

[6] Rocca, P., G. Oliveri, R. J. Mailloux, and A. Massa, "Unconventional phased array architectures and design methodologies — A review," *Proceedings of the IEEE*, Vol. 104, No. 3, 544–560, 2016.

[7] Mou, L. W., J. X. Sun, H. S. Lin, Y. Fan, and Y. J. Cheng, "Dictionary-based excitation matching convex optimization model for designing subarrayed feed array of beam-scanning reflector antenna," *IEEE Antennas and Wireless Propagation Letters*, Vol. 22, No. 12, 3112–3116, 2023.

[8] Benoni, A., L. Poli, P. Rocca, and A. Massa, "Design of clustered phased arrays by means of an innovative power pattern matching-driven method — The linear array case," *IEEE Transactions on Antennas and Propagation*, Vol. 72, No. 5, 4185–4197, 2024.

[9] Morabito, A. F., T. Isernia, M. G. Labate, M. Durso, and O. M. Bucci, "Direct radiating arrays for satellite communications via aperiodic tilings," *Progress In Electromagnetics Research*, Vol. 93, 107–124, 2009.

[10] Dong, W., Z.-H. Xu, X.-H. Liu, L.-S.-B. Wang, and S.-P. Xiao, "Irregular subarray tiling via heuristic iterative convex relaxation programming," *IEEE Transactions on Antennas and Propagation*, Vol. 68, No. 4, 2842–2852, 2020.

[11] Ma, Y., Q. Feng, Q. Jin, and Q. Xiang, "Wide-angle scanning design of irregular arrays based on unequal phase feeding," *IEEE Transactions on Antennas and Propagation*, Vol. 72, No. 5, 4129–4140, 2024.

[12] Lin, H. S., L. W. Mou, C. J. Li, and Y. J. Cheng, "A domino tiling method for circularly polarized subarrayed phased array antenna based on modified maximum-entropy model," *IEEE Transactions on Antennas and Propagation*, Vol. 72, No. 4, 3315–3324, 2024.

[13] Abdulqader, A. J., "Low complexity irregular clusters tiling through quarter region rotational symmetry," *Progress In Electromagnetics Research C*, Vol. 137, 81–91, 2023.

[14] Abdulqader, A. J., J. R. Mohammed, and Y. A. Ali, "A T-shaped polyomino subarray design method for controlling sidelobe level," *Progress In Electromagnetics Research C*, Vol. 126, 243–251, 2022.

[15] Mou, L. W. and Y. J. Cheng, "Design of aperiodic subarrayed phased arrays with structural repetitiveness," *IEEE Transactions on Antennas and Propagation*, Vol. 70, No. 12, 11 697–11 706, 2022.

[16] Anselmi, N., L. Tosi, P. Rocca, G. Toso, and A. Massa, "A self-replicating single-shape tiling technique for the design of highly modular planar phased arrays — The case of L-shaped rep-tiles," *IEEE Transactions on Antennas and Propagation*, Vol. 71, No. 4, 3335–3348, 2023.

[17] Ibrahim, N. H., A. J. Abdulqader, and J. R. Mohammed, "Configuration of hybrid clustered structures in large planar arrays for optimizing beam pattern coverage," in *2024 International Conference on Radar, Antenna, Microwave, Electronics, and Telecommunications (ICRAMET)*, 170–176, Bandung, Indonesia, 2024.

[18] Wu, Y., Y. Li, Z. Liang, S. Zheng, and Y. Long, "Reflected sidelobe suppression for periodic leaky-wave antennas with gradient structure," *IEEE Antennas and Wireless Propagation Letters*, Vol. 24, No. 7, 1854–1858, 2025.

[19] Zhu, R., J. Zhou, S. Chen, and H. Ding, "A grating and sidelobe suppression algorithm for near-field sparse periodic MIMO array imaging," *Remote Sensing Letters*, Vol. 16, No. 3, 232–242, 2025.

[20] Wu, Z., P. Wu, W. Liu, and Z. Zhang, "Adaptive subarray partitioning for large-scale phased arrays using ISODATA," *Electronics Letters*, Vol. 61, No. 1, e70212, 2025.

[21] Capozzoli, A., C. Curcio, G. D'Elia, and A. Liseno, "A technique for the array partitioning," *Radio Science*, Vol. 57, No. 10, 1–22, 2022.

[22] Zhou, J., Y. Wang, Z. Wang, C. Pang, Y. Li, and X. Wang, "Irregular subarray tiling via rotational symmetry," *IEEE Antennas and Wireless Propagation Letters*, Vol. 22, No. 4, 903–907, 2023.

[23] Anselmi, N., P. Rocca, M. Salucci, and A. Massa, "Irregular phased array tiling by means of analytic schemata-driven optimization," *IEEE Transactions on Antennas and Propagation*, Vol. 65, No. 9, 4495–4510, 2017.